arXiv:1601.04394v1 [astro-ph.HE] 18 Jan 2016

Search for Soft X-ray Flashes at Fireball Phase of Classical/Recurrent Novae using MAXI/GSC data

Mikio MORII[1], Hitoshi YAMAOKA[2], Tatehiro MIHARA[3], Masaru MATSUOKA[3] and Nobuyuki KAWAI[4]

[1]Research Center for Statistical Machine Learning, The Institute of Statistical Mathematics, & Core Research for Evolutionary Science and Technology (CREST), Japan Science and Technology Agency (JST), 10-3 Midori-cho, Tachikawa, Tokyo 190-8562, Japan

[2]Department of Physics, Kyushu University, 6-10-1 Hakozaki, Fukuoka-shi Higashi-ku, Fukuoka 812-8581, Japan

[3]MAXI Team, Institute of Physical and Chemical Research (RIKEN), 2-1 Hirosawa, Wako, Saitama 351-0198, Japan

[4]Department of Physics, Tokyo Institute of Technology, Ookayama 2-12-1, Meguro-ku, Tokyo 152-8551, Japan

*E-mail: morii@ism.ac.jp

Received 2015 September 28; Accepted 2016 January 17

Abstract

We searched for precursive soft X-ray flashes (SXFs) associated with optically-discovered classical or recurrent novae in the data of five-years all-sky observations with Gas Slit Camera (GSC) of the Monitor of All-sky X-ray Image (MAXI). We first developed a tool to measure fluxes of point sources by fitting the event distribution with the model that incorporates the point-spread function (PSF-fit) to minimize the potential contamination from nearby sources. Then we applied the PSF-fit tool to 40 classical/recurrent novae that were discovered in optical observations from 2009 August to 2014 August. We found no precursive SXFs with significance above 3σ level in the energy range of 2$-$4 keV between $t_d - 10$d and t_d, where t_d is the date when each nova was discovered. We obtained the upper limits for the bolometric

luminosity of SXFs, and compared them with the theoretical prediction and that observed for MAXI J0158−744. This result could constrain the population of massive white dwarfs with a mass of roughly 1.40 solar mass, or larger, in binary systems.

Key words: (stars:) novae, cataclysmic variables; (stars:) white dwarfs; X-rays: bursts; methods: data analysis

1 Introduction

Both classical and recurrent novae are triggered by thermonuclear runaways, which last for $\sim$100 s at the surface of white dwarfs. Subsequently, the optical flux increases by 6 or more magnitudes, followed by an eventual decline to quiescence (Warner 1995). At the time of thermonuclear runaways, an emission in the ultraviolet to soft X-ray bands that lasts for only a few hours is predicted and is called "fireball phase" (Starrfield et al. 2008; Krautter 2008). The fireball phase is predicted to happen a few days before the beginning of the optical nova phase, although it has not been detected yet from any nova system.

In fact, MAXI/GSC did discover an extraordinarily luminous soft X-ray flash (SXF) MAXI J0158−744 (Li et al. 2012; Morii et al. 2013). The MAXI J0158−744 system was considered to be in the fireball phase, although there was no association with a usual classical/recurrent nova. This SXF is characterized with a soft X-ray spectrum, a short duration (ΔT_d; 1.3×10^3 s $< \Delta T_d < 1.10 \times 10^4$ s), a rapid rise ($< 5.5 \times 10^3$ s), and a huge peak luminosity of 2×10^{40} erg s^{-1} in the $0.7 - 7.0$ keV band. Although the characteristics of this flash are very different from those of usual novae, the soft X-ray emission was successfully interpreted as the fireball phase of a new kind of novae on a very massive white dwarf (Morii et al. 2013). Indeed, this hypothesis was further supported with a detailed simulation performed by Ohtani, Morii & Shigeyama (2014). The soft X-ray emission during the fireball phase is a photospheric emission, and accordingly, the spectral shape is basically a blackbody. Morii et al. (2013) also concluded that the small increase in the flux observed in the optical counterpart of MAXI J0158−744 did not originate from a photospheric emission as usual novae, but is due to the emission from the disk around the Be companion star, which is a reprocess, originated from the photospheric soft X-ray emission. Now, unlike MAXI J0158−744, the companion star in the white-dwarf binaries that generate novae is in general not a Be star. Then, it is unlikely any detectable increase in the optical flux would occur during SXF of a nova, where the companion star is not a Be star.

It has been argued in many theoretical studies that white dwarfs can acquire a mass close to or over the Chandrasekhar limit via differential rotation (e.g. Yoon & Langer (2004) and Hachisu et al. (2012)) or strong internal magnetic fields (e.g. Das & Mukhopadhyay (2012) and Franzon & Schramm (2015)). However, the theoretical works have not caught up with the observational discovery of the new type of nova from a very massive white dwarf (MAXI J0158−477; Morii et al. (2013)). At the same time, we need more observational samples to study and understand the phenomenon and its background science. Here we present the result of the systematic search for nova explosions from very massive white dwarfs.

In this paper, we perform the systematic search for the fireball phase emission in the soft X-ray band for usual classical/recurrent novae, using the association of optically discovered novae as predicted by Starrfield et al. (2008) and Krautter (2008). We should note that the SXF without optical-nova phase like MAXI J0158−744 are out of our samples and hence would not be detected in this search. However, intermediate objects that possess both the fireball phase with a SXF emission and a optical nova phase are expected to be found, if such objects are actually present.

2 Observation and Analysis

MAXI (Monitor of All-sky X-ray Image; Matsuoka et al. 2009) is an all-sky X-ray monitor, which is operated on the Japanese Experiment Module (KIBO) on the International Space Station (ISS). MAXI carries Gas Slit Camera (GSC; Mihara et al. 2011; Sugizaki et al. 2011), which scans the almost entire sky every ~ 92 minutes through the long and narrow fields of view (FoVs) of $1.^{\circ}5 \times 160^{\circ}$. The scan duration for a point source is $40 - 150$ s (Sugizaki et al. 2011). GSC with its gas proportional counters is sensitive for $2 - 30$ keV. From the start of the operation on 2009 August 15 up to the present day, GSC has almost continuously monitored the whole sky. All the data have been stored in Japan Aerospace Exploration Agency (JAXA) and Institute of Physical and Chemical Research (RIKEN).

Table 1 shows the classical/recurrent novae discovered in the period from 2009 August 15 to 2014 August 15, taken from the reports of the International Astronomical Union Circulars (IAUC) and Central Bureau Electronic Telegrams (CBET). MAXI/GSC observed these fields of the sky at the period of the discovery in the optical wavelength. Accordingly, MAXI/GSC can search the precursive activity in the X-ray band for these novae.

We started the data analysis from the event data of MAXI/GSC stored in every day and every camera in the `fits` format. For every source, we extracted events from a circular sky region centered on the target with a radius of 8°, using `mxextract`. We also calculated the time variation of the

effective area in every 1 s for the point source determined by slat-slit collimator of MAXI/GSC, using `mxscancur`. We made good time intervals (GTIs) to include this duration and to remove the duration when the counter was off. We also removed the scans during which the solar paddle of the ISS obscured the FoV of the GSC counter. The selected event data in `fits` format were converted to `root` [1] format to enhance visualization of the data. For every scan, we measured the flux of the target in the unit of counts s^{-1} cm^{-2} in the $2-4$ keV band, using the tool named "PSF-fit". The details of the "PSF-fit" are described in Appendix 1. The spectrum file and the corresponding response file were made for every scan by using `xselect` and `mxgrmfgen`, respectively.

We made the light curves of the sources listed in Table 1 in every GSC scan, using the PSF-fit tool from $t_d - 50$ d to $t_d + 50$ d, where t_d is the time, when each nova was discovered in the optical wavelength. We also calculated the upper limits for the fluxes in 90% confidence level (C.L.) for the scans with non-detection, using the same tool.

3 Results

For every nova listed in Table 2, no significant precursive SXF was found at more than 3σ level during the period between $t_d - 10$d and t_d. Note that in this table, U Sco, V1310 Sco, V5666 Sgr and V745 Sco listed in Table 1 are removed due to the following reasons. U Sco is removed due to the occasional contamination of the tail of the PSF of Sco X-1. Although the angular distance between them is not so small (2.4 deg), Sco X-1 is the brightest X-ray source in the entire sky (~ 10 Crab), then the contamination becomes sometimes severe. V1310 Sco is also removed due to the contamination of the nearby bright source GX 349+2, which is 0.8 deg apart from V1310 Sco. For V5666 Sgr and V745 Sco, there was no GTI of GSC scans during the searched periods.

We then calculated the 90%C.L. upper limit for the fluxes in every scan for the sources in the unit of counts s^{-1} cm^{-2} in the $2-4$ keV band (Table 2). Since the expected times of the SXFs are unknown, the upper limits given in the table are the averaged values for all the scans between $t_d - 10$d and t_d, as well as the minimum and maximum. From these averaged flux upper-limits, we calculated the upper limits for bolometric luminosity of the sources, using the interstellar absorption N_H and the distance (Table 2), and assuming the temperature of blackbody spectrum for the fireball-phase emission. Figure 1 shows the derived upper limits.

[1] https://root.cern.ch/drupal/

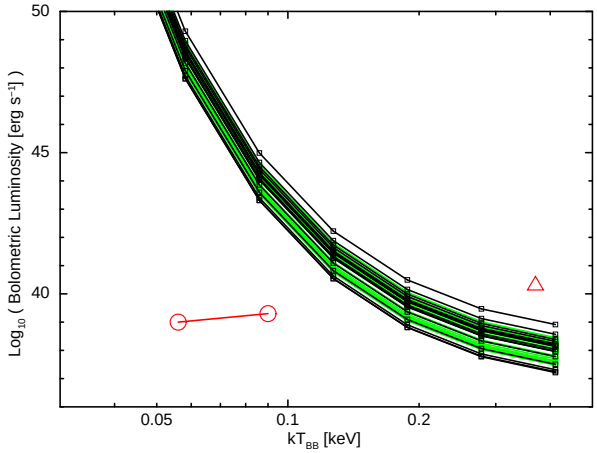

Fig. 1. The 90% C.L. upper limits for bolometric luminosity of the fireball phase of classical/recurrent novae searched for in this work (see Table 2). In the conversion from the observed GSC flux in the $2-4$ keV band (counts s^{-1} cm^{-2}) to the unabsorbed bolometric luminosity (erg s^{-1}), a blackbody spectrum is assumed, and the interstellar absorption N_H and distance listed in Table 2 are used. For the sources with unknown distance, we assumed 5 kpc as a typical distance for Galactic sources. The upper limits for the sources with known and unknown distances are shown in black and green lines, respectively. Horizontal and vertical axes are the temperature of blackbody assumed in the flux conversion in the units of keV and logarithm of bolometric luminosity, respectively. The theoretical prediction of the fireball phase (Starrfield et al. 2008) is given in red circle points connected with a solid line, to be compared with the derived upper limits, where the left and right circle-points correspond to the emission in the fireball phase of white dwarfs with respective 1.25 and 1.35 solar masses. The red triangle point is the observed value for the fireball phase on MAXI J0158−744 (Morii et al. 2013).

4 Discussion and Conclusion

If SXFs are associated precursively with optical novae, if the spectrum and flux are similar to those of MAXI J0158−744, and if the nova is located at the typical distance of 5 kpc, then MAXI/GSC should detect these flashes in high significance (see Figure 1), as long as the FoV of GSC covers the direction during the SXF. MAXI/GSC usually scans a specific direction every 92 minutes. Hence, the probability that MAXI/GSC detects a SXF depends on the duration of the SXF.

In our study, we performed $n = 40$ trials of MAXI/GSC observations for SXFs and found no detection. Statistically speaking, our experiment is a sequence of independent Bernoulli trials with a success probability of $Rp_c^{(i)}$, where R is the fraction of novae associated with SXF at the fireball phase and $p_c^{(i)}$ is the probability for MAXI/GSC to scan the direction of the i-th nova during the search period between $t_d - 10$ d and t_d. By denoting the detection or non-detection for the i-th trial as $d_i = 1$ or 0, respectively, the joint probability of $\mathbf{d}$ throughout this experiment is given by

$$P(\mathbf{d}; R, \mathbf{p_c}) = \prod_{i=1}^{n} (Rp_c^{(i)})^{d_i} (1 - Rp_c^{(i)})^{1-d_i}, \quad (1)$$

where $\mathbf{d} = (d_1, \cdots, d_n)$ and $\mathbf{p_c} = (p_c^{(1)}, \cdots, p_c^{(n)})$ are vectors of the detection and the probability, respectively. Following our result of non-detection ($\mathbf{d} = \mathbf{0}$), we calculated the upper limit for the fraction R to be in 90% confidence level, varying the duration of the SXF. Figure 2 shows this upper limit as a function of the duration of the SXF, where the limit was calculated with the standard method

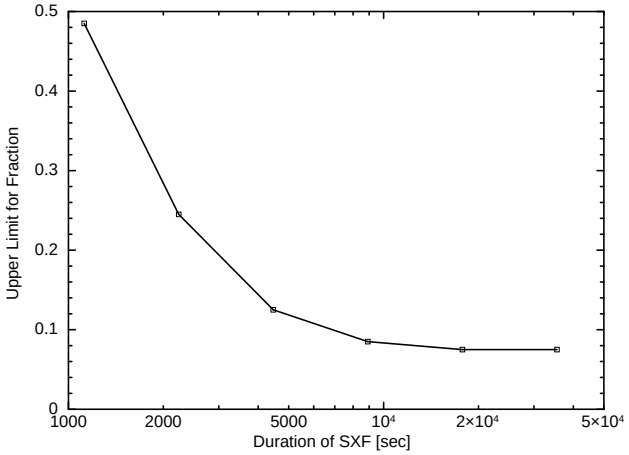

Fig. 2. The 90% C.L. upper limit for the fraction of novae associated with a SXF at the fireball phase (R) as a function of the given duration of SXFs in the unit of second (see text).

of interval estimation of a parameter by inverting a likelihood-ratio test-statistic (Section 9.2 in Casella & Berger 2002). Note that we evaluated the probability distribution of the function in Equation 1 with Monte Carlo simulation in the calculation.

In Figure 1, the fireball phase observed on MAXI J0158−744 is located at the extension of theoretical prediction (Starrfield et al. 2008). It supports that the SXF observed on MAXI J0158−744 is the emission from the fireball phase. The mass of the white dwarf of this source is estimated to be at least 1.35 solar mass. Furthermore, by naively drawing a straight line connecting the two points of 1.35 solar mass (the right red circle) and MAXI J0158−744 (red triangle), the crossing point between this line and the average of the lines of the upper limits implies a lower limit for the mass of white dwarfs for which the SXFs are detectable with MAXI/GSC. Assuming that the mass of MAXI J0158−744 is at the Chandrasekhar limit of white dwarfs (1.44 solar mass), the mass of a white dwarf that is located at the crossing point is estimated to be about 1.40 solar mass. Therefore, the upper limit for the fraction in Figure 2 can be alternatively interpreted as the upper limit for the population of white dwarfs in binary systems whose masses are about 1.40 solar mass or larger. The population of very massive white dwarfs is important for estimating the rate of type Ia supernovae. Our result could give a constraint for this population.

Future observations with MAXI/GSC will detect more SXFs from novae in the fireball phases. In addition, wide-field MAXI mission under planning (Kawai et al. 2014) would improve the detection efficiency of SXFs and would increase the sample of SXFs and very massive white dwarfs. In the light of these prospects, the theoretical study of the fireball-phase emission of novae on very massive white dwarfs, especially from 1.35 solar mass to near the Chandrasekhar limit, is encouraged.

Acknowledgments

We thank the member of the MAXI operation team. We also thank J. Shimanoe for the first search for transients from optical novae. K. Sugimori, T. Toizumi and T. Yoshii kindly offered us a good help in developing the PSF-fit. We are grateful for S. Ikeda on ISM, who advised for the statistical treatment of the data analysis. This work was partially supported by the Ministry of Education, Culture, Sports, Science and Technology (MEXT), Grant-in-Aid for Science Research 24340041.

Appendix 1 Flux measurement by using the point-spread function — PSF-fit

X-ray fluxes of point sources are usually measured with aperture photometry, and the standard processing for the MAXI data too follows it. The MAXI light-curves obtained with this method are published in the archive on the website of RIKEN [2]. In the standard MAXI data-processing, the source and background regions to extract events are selected usually as simple circular and annulus regions in the sky coordinates, respectively. When the point-spread functions (PSFs) of nearby sources interfere these regions, the circular regions centered on these nearby sources are excluded. If a target source is located in a severely crowded region like the Galactic plane, measurement of the flux based on such a simple selection of the regions is inadequate, because the PSF of a target overlaps with those of nearby sources and because the area of the background region free from contamination of the nearby sources becomes too small to obtain the adequate statistics.

In this work, we developed a tool to measure the fluxes for the point sources by fitting event distribution around a target with a model that incorporates of the PSFs of the target and nearby sources. Both X-ray and non-X-ray backgrounds are also taken into account in this model. We name this tool the PSF-fit. The following is the detailed description of the PSF-fit.

We use event distribution in the detector coordinate rather than the sky coordinate, because the shape of a PSF is best described in the detector coordinate. In this coordinate, the shape of a PSF is given by a triangular-shaped function in the time (scan) direction, whereas that in the anode wire direction is given by a Gaussian shape (Sugizaki et al. 2011). The triangular shape is well calibrated (Morii, Sugimori & Kawai 2011). The width of the Gaussian shape (sigma) depends on counters, the position of the anode direction, and the high voltage (HV; 1650V or 1550V). We calibrated this dependence by measuring the width of the Gaussian shape for the bright point sources, Crab nebula, GRS 1915+105, and Cyg X-1, for the energy bands of $2-4$ and $4-10$ keV. Thus, we obtained the well-calibrated PSF model.

We modeled the event distribution in the detector coordinate (t, b) of a camera ($k = 0, \cdots, 11$; camera IDs) as follows:

[2] http://maxi.riken.jp/top/

$$F_{\rm model}(t,b;k) = \sum_{m\in S_k} f^{(m)} g^{(m)}_{\rm psf}(t,b;\alpha_m,\delta_m,k) + B(t,b;k), \tag{A1}$$

where t is time (s), b is the position of anode, bex (mm), and (α_m, δ_m) are the sky coordinates (Right ascension, Declination) of the target and nearby sources. S_k is a set of sources, including the target and nearby sources (m: source IDs), and they are different among cameras (k), because the FoVs and condition of each camera are different. $f^{(m)}$ and $g^{(m)}_{\rm psf}(t,b)$ are the source flux in the unit of counts s^{-1} cm^{-2} and the shape of the PSF in the unit of cm^2 mm^{-1}. $B(t,b;k)$ is the shape of a background rate in the unit of counts s^{-1} mm^{-1}, for which we used a constant function in this study.

We select events from a rectangular region in the detector coordinate, where the width of time (scan) direction is determined to be three times the width of the base side of the triangular shape. That of the anode direction is set to be 16 sigma of the Gaussian shape. As a result, these widths vary in every scan. We then add a constraint for these widths so that the rectangular region cannot exceed a circular sky region with a radius of 8 deg, which is the radius of the event extraction at the beginning of the analysis (Section 2). Figure 3 shows an example of the event distribution in the detector coordinate to be used for the PSF-fit. It is for V5586 Sgr on a scan at the modified Julian day (MJD) 55340 with a camera (ID = 0) in the $2-4$ keV band.

We minimize the following cost function, c-stat (Cash 1979), to calculate the fluxes of a target and nearby sources,

$$\begin{aligned} c &= \sum_{k\in A} c_k = -2\sum_{k\in A} \ln L_k \\ &= -2\sum_{k\in A}\left[\sum_{i\in E_k} \ln F_{\rm model}(t_i,b_i;k) \right. \\ &\quad \left. - \int_{\rm M_k} F_{\rm model}(t,b;k)\,dt\,db\right], \end{aligned} \tag{A2}$$

where A is a set of the operating cameras and E_k is a set of the events detected in a camera (k). M_k is an integration area for a camera (k), where the time duration of HV-off and the center of the camera in the anode direction ($|b| < 4$ mm) are masked out. The region of the anode edges ($|b| > 130$ mm) is also masked out. To speed up the calculation, we use unbinned likelihood instead of binned likelihood. `Minuit2` [3] minimizer is used for minimization of the cost function. To calculate the error ranges, we calculate the likelihood interval (Cowan 1998), using `minos` in `Minuit2`.

When a target is located in a crowded region like the Galactic plane, there are many various nearby sources; some sources are always bright enough to be detected by MAXI/GSC, while some are usually faint and have a potential to become bright above the threshold of MAXI/GSC sensitivity. For almost any region in the sky, MAXI/GSC is the only X-ray detector that monitors these sources;

[3] http://seal.web.cern.ch/seal/snapshot/work-packages/mathlibs/minuit/

then it is impossible to determine a priori which sources are detectable and which are not. However, we must select which source is necessary to be included in the model for the PSF-fit. We approach this problem as follows.

We pick up candidates for the nearby sources to be included in the PSF-fit from the catalog used in the Nova search system (Negoro et al. 2015). The area for picking up these candidates are the rectangular region in the detector coordinate as described above and the outer marginal region with half width of the base side of the triangular shape for the time direction and three sigma of the Gaussian shape for the anode direction. This marginal region for selecting the nearby sources is necessary to account for the contamination of PSFs of sources out of the fitting region, within which the events are extracted (Figure 3). Figure 4 demonstrates the positions of the nearby candidate sources listed in the catalog in the example case, as well as the region for the event extraction (fitting) and outer marginal regions.

The nearby sources included in the PSF-fit (black labels in Figure 4) are selected with the measure of the Bayesian information criterion (BIC; Schwarz 1978) from the candidates (green labels in Figure 4) as follows. First, we fit the event distribution with the simplest model that includes only the background, and calculate the BIC. Next, we include one nearby source among all the nearby candidate sources into the model function, and fit the events with this model and calculate the BIC. We then identify the best nearby source with the minimum BIC as the first selected nearby source. If this minimum BIC is larger than that of the previous BIC obtained by the fit that includes only the background, which means that no nearby source is necessary to improve the fit, then the model selection for the nearby sources is completed. Otherwise, we include this source in the final model, then proceed to the next step. In the next step, we include another nearby source among the rest of the nearby sources, and repeat the above procedure. We stop this procedure when the BIC reaches the minimum. Finally, we add the target source in the final model. Figure 4 demonstrates the positions of nearby sources selected with this model selection, and these are used for the fitting process.

Figures 5, 6 and 7 show an example of the best-fit model obtained with the PSF-fit tool; they show the model function, and the projection onto the time and anode directions, respectively.

To demonstrate the efficacy of the PSF-fit, we present Figure 8. It shows a light curve of a moderately bright and stable source 4U 1746−37. Due to a periodic contamination of the tail of the PSF of a nearby bright source, the light curve available on the website of RIKEN is disturbed with a periodic artificial modulation caused by the precession of the ISS (top panel). With the PSF-fit, this modulation effect is clearly removed (bottom panel).

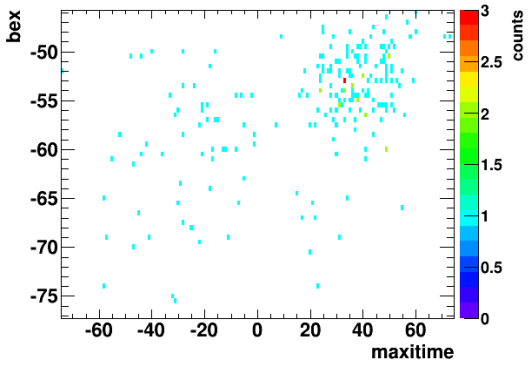

Fig. 3. Event distribution in the detector coordinate extracted for the PSF-fit for V5586 Sgr on a scan at MJD 55340 by a camera (ID = 0) in the $2-4$ keV band. Horizontal and vertical axes are the relative time(s) from 2010-05-24 15:34:14 (UT) and bex (mm), respectively. The color scale shows the number of events in a bin.

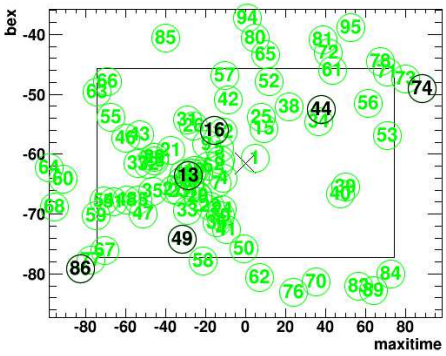

Fig. 4. The positions of the nearby source candidates and the selected sources are shown in numerical labels with green and black colors, respectively. The cross label at the center is the position of the target, V5586 Sgr. The scan time and camera are the same as in Figure 3. The area used for the PSF-fit is displayed as a rectangular region, which is the same area as that in Figure 3.

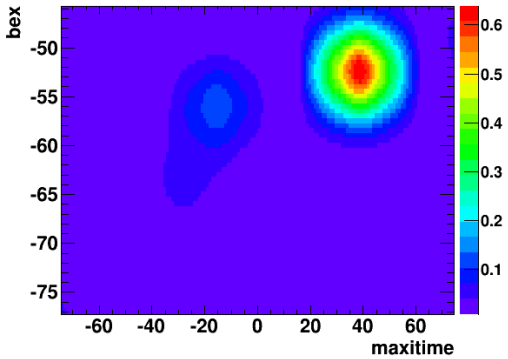

Fig. 5. The best-fit function obtained with the PSF-fit for the same region as in Figure 3. The value of the best-fit function are shown in the unit of counts s^{-1} mm^{-1} (color bar).

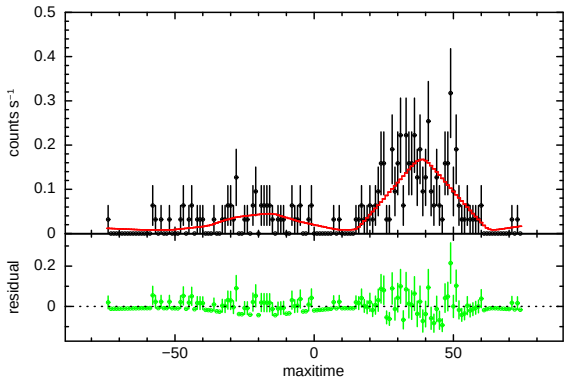

Fig. 6. (Top panel:) The projection of the best-fit function in Figure 5 onto the time direction (red histogram). The same projection of the event distribution of Figure 3 is given in crosses. The vertical axis is the event rate in the unit of counts s^{-1}. (Bottom panel:) The residual of the best-fit.

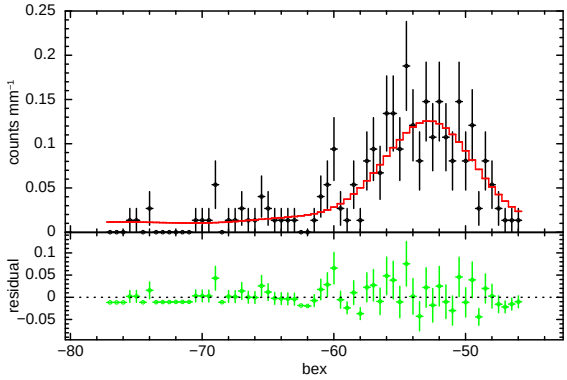

Fig. 7. (Top panel:) The projection of the best-fit function in Figure 5 onto the anode direction (red histogram). The same projection of the event distribution of Figure 3 is given in crosses. The vertical axis is the event rate in the unit of counts mm^{-1}. (Bottom panel:) The residual of the best-fit.

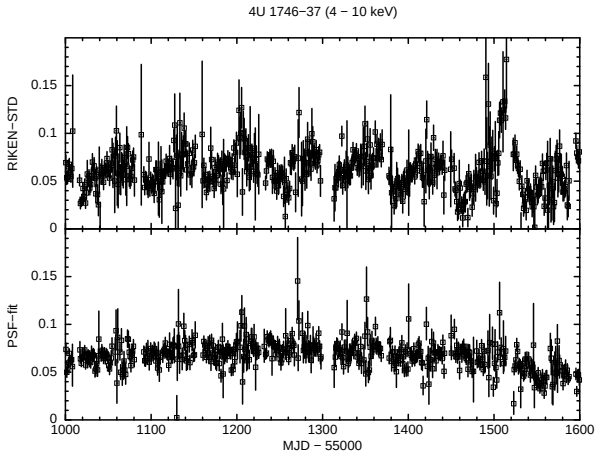

Fig. 8. The light curves of 4U 1746-37 in the $4-10$ keV band in one-day bins in the unit of counts s^{-1} cm^{-2}. Horizontal axis is in days (MJD - 55000). The top panel shows the light curve in the data archive at the RIKEN web site, whereas the bottom panel is that obtained with the PSF-fit.

References

Ackermann, M. et al. 2014, Science, 345, 554

Casella, G. & Berger, R. L. 2002, “Statistical Inference”, 2nd. Ed., Brooks/Cole, Cengage Learning.

Cash, W. 1979, ApJ, 228, 939

Cowan, G. 1998, “Statistical Data Analysis”, Oxford Science Publications

Das, U. & Mukhopadhyay, B. 2012, Physical Review D, 86, 042001

Dickey, J. M., & Lockman, F. J. 1990, ARA&A, 28, 215

Franzon, B. & Schramm, S. 2015, Physical Review D, 92, 083006

Hachisu, I., Kato, M., Saio, H., & Nomoto, K. 2012, ApJ, 744, 69

Imamura, K. & Tanabe, K. 2012, PASJ, 64, 120

Joshi, V. et al. 2015, MNRAS, 452, 3696

Kalberla, P. M. W. et al. 2005, A&A, 440, 775

Kawai, N. et al. 2014, Proceedings of the SPIE, 9144, 91442P

Krautter, J. 2008, in X-ray Emission from Classical Novae in Outburst in Classical Novae, ed. M. Bode & A. Evans (2nd ed.; Cambridge: Cambridge Univ. Press), 232

Li, K. L. et al. 2012, ApJ, 761, 99

Matsuoka, M. et al. 2009, PASJ, 61, 999

Mihara, T. et al. 2011, PASJ, 63, S623

Morii, M., Sugimori, K., & Kawai, N. 2011, Physica E: Lowdimensional Systems and Nanostructures, 43, 692

Morii, M. et al. 2013, ApJ, 779, 118

Munari, U. et al. 2010, PASP, 122, 898

Munari, U. et al. 2014, MNRAS, 440, 3402

Munari, U. et al. 2015, MNRAS, 447, 1661

Munari, U. & Dallaporta, S. 2010, Information Bulletin on Variable Stars, 5932, 1.

Munari, U., Dallaporta, S. & Ochner, P. 2010, Information Bulletin on Variable Stars, 5944, 1

Munari, U., Margoni, R. & Stagni, R. 1990, MNRAS, 242, 653

Negoro, H. et al. 2015, PASJ, this special volume.

Ohtani, Y, Morii, M. & Shigeyama, T. 2014, ApJ, 787, 165

Raj, A. et al. 2015, Research in Astronomy and Astrophysics, 15, 993

Raj, A. et al. 2012, MNRAS, 425, 2576

Schaefer, B. E. 2010, ApJS, 187, 275

Schwarz, G. E. 1978, Annals of Statistics, 6, 461

Shore, S. N. 2013, ATel, 5410

Shore, S. N. et al. 2013, A&A, 553, 123

Shore, S. N. 2014, ATel, 6413

Starrfield, S., Iliadis, C., & Hix, W. R. 2008, in Thermonuclear Processes in Classical Novae, ed. M. Bode & A. Evans (2nd ed.; Cambridge: Cambridge Univ. Press), 77

Sugizaki, M. et al. 2011, PASJ, 63, S635

Takei, D. et al. 2014, PASJ, 66, 37

Warner, B. 1995, Novae in Eruption in Cataclysmic Variable Stars (Cambridge: Cambridge Univ. Press)

Weston, J. H. S. et al. 2015, submitted to MNRAS (arXiv:1505.05879)

Yoon, S.-C., & Langer, N. 2004, A&A, 419, 623

Table 1. Forty-four classical/recurrent novae discovered in the optical wavelengths during five years from 2009 August to 2014 August

Nova	R.A.[1]	Dec.[2]	Discovery	Class[3]	Reference[4]
	deg	deg	Date (UT)[5]		
V2672 Oph	264.582	−26.737	2009-08-16.515	CN	IAUC 9064
V5584 Sgr	277.887	−16.319	2009-10-26.439	CN	IAUC 9089
V496 Sct	280.940	−7.612	2009-11-08.370	CN	IAUC 9093, CBET 2008
KT Eri	71.976	−10.179	2009-11-25.545	CN	IAUC 9098
V1722 Aql	288.541	+15.276	2009-12-14.40	CN	IAUC 9100
V2673 Oph	264.921	−21.663	2010-01-15.857	CN	IAUC 9111
V5585 Sgr	271.862	−29.012	2010-01-20.72	CN	IAUC 9112
U Sco	245.628	−17.879	2010-01-28.4385	RN	IAUC 9111
V2674 Oph	261.634	−28.827	2010-02-18.845	CN	IAUC 9119
V1310 Sco	256.531	−37.241	2010-02-20.857	CN	IAUC 9120
V407 Cyg	315.541	+45.776	2010-03-10.797	SyN	CBET 2199
V5586 Sgr	268.262	−28.205	2010-04-23.782	CN	IAUC 9140
V1311 Sco	253.805	−38.063	2010-04-25.788	CN	IAUC 9142
V1723 Aql	281.910	−3.787	2010-09-11.485	CN	IAUC 9167
V5587 Sgr	266.943	−23.587	2011-01-25.86	CN	IAUC 9196
V5588 Sgr	272.589	−23.092	2011-03-27.832	CN	IAUC 9203, CBET 2679
T Pyx	136.173	−32.380	2011-04-14.2931	RN	IAUC 9205, CBET 2700
V1312 Sco	253.789	−38.635	2011-06-01.40	CN	IAUC 9216, CBET 2735
PR Lup	223.583	−55.084	2011-08-04.73	CN	IAUC 9228, CBET 2796
V1313 Sco	249.179	−41.546	2011-09-06.37	CN	IAUC 9233, CBET 2813
V965 Per	47.818	+37.084	2011-11-07.75	CN	IAUC 9247
V834 Car	162.582	−64.113	2012-02-26.543	CN	IAUC 9251, CBET 3040
V1368 Cen	205.289	−58.255	2012-03-23.386	CN	IAUC 9260, CBET 3073
V2676 Oph	261.529	−25.862	2012-03-25.789	CN	IAUC 9259, CBET 3072
V5589 Sgr	266.367	−23.090	2012-04-21.01123	CN	IAUC 9259, CBET 3089
V5590 Sgr	272.766	−27.291	2012-04-23.689	CN	IAUC 9259, CBET 3140
V2677 Oph	264.983	−24.795	2012-05-19.484	CN	IAUC 9260, CBET 3124
V1324 Sco	267.725	−32.622	2012-05-22.80	CN	CBET 3136
V5591 Sgr	268.107	−21.439	2012-06-26.5494	CN	IAUC 9259, CBET 3156
V5592 Sgr	275.114	−27.741	2012-07-07.4986	CN	IAUC 9259, CBET 3166

Table 1. (Continued)

V5593 Sgr	274.904	−19.128	2012-07-16.512	CN	IAUC 9259, CBET 3182
V959 Mon	99.911	+5.898	2012-08-07.8048	CN	IAUC 9259, CBET 3202
V1724 Aql	283.146	+0.312	2012-10-20.4294	CN	IAUC 9259, CBET 3273
V809 Cep	347.020	+60.781	2013-02-02.4119	CN	IAUC 9260, CBET 3397
V1533 Sco	263.498	−36.106	2013-06-03.6146	CN	IAUC 9260, CBET 3542
V339 Del	305.878	+20.768	2013-08-14.5843	CN	IAUC 9258, CBET 3628
V1830 Aql	285.639	+3.255	2013-10-28.4571	CN	IAUC 9263, CBET 3691, CBET 3708
V556 Ser	272.264	−11.210	2013-11-24.3835	CN	IAUC 9264, CBET 3724
V1369 Cen	208.696	−59.152	2013-12-02.692	CN	IAUC 9265, CBET 3732
V5666 Sgr	276.286	−22.601	2014-01-26.857	CN	IAUC 9269, CBET 3802
V745 Sco	268.843	−33.250	2014-02-06.694	RN	CBET 3803
V962 Cep	313.599	+60.285	2014-03-08.7917	CN	IAUC 9270, CBET 3825
V1534 Sco	258.945	−31.475	2014-03-26.8487	CN	IAUC 9273, CBET 3841
V2659 Cyg	305.426	+31.058	2014-03-31.7899	CN	IAUC 9271, CBET 3842

[1]Right ascension. [2]Declination.

[3]CN: Classical Nova; RN: Recurrent Nova; SyN: Symbiotic Nova

[4]IAUC: The International Astronomical Union Circulars,

CBET: Central Bureau Electronic Telegrams

[5](Year)-(Month)-(Day)

Table 2. Results of our search for soft X-ray flashes for the forty novae in Table 1

Nova[1]	$N_{\rm H}$[2]	Distance	U.L.[3]	$N_{\rm s}$[4]	Reference for distance
	$\rm cm^{-2}$	kpc	ave (min – max)		
V2672 Oph	4.18×10^{21}	19 ± 2	2.51 (0.71 – 4.24)	22	Takei et al. (2014)
V5584 Sgr	3.96×10^{21}	6.3 ± 0.5	1.20 (0.38 – 3.28)	134	Raj et al. (2015)
V496 Sct	6.81×10^{21}	2.9 ± 0.3	2.22 (0.74 – 4.75)	45	Raj et al. (2012)
KT Eri	5.52×10^{20}	6.6 ± 0.8	1.71 (0.61 – 6.03)	109	Imamura & Tanabe (2012)
V1722 Aql	9.14×10^{21}	5	1.97 (0.63 – 6.01)	112	Munari et al. (2010)
V2673 Oph	2.84×10^{21}	7.4	1.42 (0.43 – 4.38)	77	Munari & Dallaporta (2010)
V5585 Sgr	2.75×10^{21}	N/A	1.76 (0.50 – 4.36)	44	
V2674 Oph	4.12×10^{21}	9	1.75 (0.67 – 3.96)	30	Munari, Dallaporta & Ochner (2010)
V407 Cyg	8.19×10^{21}	2.7	1.83 (0.56 – 4.46)	52	Munari, Margoni, & Stagni (1990)
V5586 Sgr	9.60×10^{21}	N/A	2.79 (1.21 – 5.64)	23	
V1311 Sco	4.78×10^{21}	N/A	1.98 (0.52 – 4.44)	20	
V1723 Aql	1.23×10^{22}	6	1.76 (0.49 – 4.97)	140	Weston et al. (2015)
V5587 Sgr	4.09×10^{21}	N/A	1.56 (0.30 – 3.67)	126	
V5588 Sgr	5.47×10^{21}	7.6	2.15 (0.65 – 5.67)	122	Munari et al. (2015)
T Pyx	1.88×10^{21}	3.5 ± 1	1.87 (0.43 – 8.19)	35	Schaefer (2010)
V1312 Sco	5.14×10^{21}	N/A	1.61 (0.47 – 4.64)	118	
PR Lup	4.82×10^{21}	N/A	1.25 (0.39 – 3.76)	144	
V1313 Sco	4.77×10^{21}	N/A	1.09 (0.26 – 3.71)	55	
V965 Per	1.20×10^{21}	N/A	3.56 (1.37 – 8.18)	17	
V834 Car	4.98×10^{21}	N/A	1.49 (0.38 – 5.09)	121	
V1368 Cen	4.30×10^{21}	N/A	1.37 (0.46 – 3.50)	47	
V2676 Oph	3.02×10^{21}	N/A	1.34 (0.36 – 3.56)	89	
V5589 Sgr	3.35×10^{21}	N/A	2.21 (0.47 – 5.85)	111	
V5590 Sgr	2.64×10^{21}	N/A	2.19 (0.70 – 5.50)	107	
V2677 Oph	3.38×10^{21}	N/A	3.46 (0.79 – 11.27)	44	
V1324 Sco	4.35×10^{21}	4.5	2.56 (0.79 – 6.05)	47	Ackermann et al. (2014)
V5591 Sgr	4.27×10^{21}	N/A	2.31 (0.61 – 6.59)	134	
V5592 Sgr	1.49×10^{21}	N/A	2.01 (0.72 – 5.96)	93	
V5593 Sgr	6.54×10^{21}	N/A	2.31 (0.66 – 5.97)	115	
V959 Mon	6.29×10^{21}	3.6	2.68 (0.71 – 9.77)	118	Shore et al. (2013)

Table 2. (Continued)

V1724 Aql	1.47×10^{22}	N/A	2.49 (0.61 – 7.11)	133	
V809 Cep	8.22×10^{21}	6.5	1.98 (0.65 – 5.25)	93	Munari et al. (2014)
V1533 Sco	7.42×10^{21}	N/A	2.10 (0.66 – 4.36)	84	
V339 Del	1.36×10^{21}	4.2	2.04 (0.64 – 6.08)	140	Shore (2013)
V1830 Aql	1.23×10^{22}	N/A	3.08 (0.86 – 8.20)	128	
V556 Ser	4.87×10^{21}	N/A	2.54 (0.93 – 6.70)	89	
V1369 Cen	5.84×10^{21}	2.4	2.58 (0.74 – 8.95)	83	Shore et al. (2014)
V962 Cep	3.30×10^{21}	N/A	2.72 (1.11 – 11.86)	125	
V1534 Sco	3.88×10^{21}	13	1.77 (0.79 – 4.24)	22	Joshi et al. (2015)
V2659 Cyg	4.92×10^{21}	N/A	2.27 (0.73 – 6.13)	124	

[1]U Sco, V1310 Sco, V5666 Sgr and V745 Sco listed in Table 1 are removed (see text).

[2]Total Galactic HI column density toward the source as the average

of the values obtained by Leiden/Argentine/Bonn (LAB) map(Kalberla et al. 2005)

and DL map (Dickey & Lockman 1990), calculated using HEASARC Web site:

http://heasarc.gsfc.nasa.gov/cgi-bin/Tools/w3nh/w3nh.pl

[3]90%C.L. upper limit for the flux in the $2-4$ keV band for each scan in the unit of 10^{-2} counts s^{-1} cm^{-2}.

Average (minimum and maximum) fluxes among N_s scans are shown.

[4]Number of GSC scans in the searched period.